Acta Crystallographica Section B
Structural Science
ISSN 0108-7681

Single-crystal study of the m = 2 tubular cobalt oxide, $Bi_4Sr_{12}Co_8O_{30-\delta}$

O. Perez,[a]* A. C. Masset,[a] H. Leligny,[a] G. Baldinozzi,[b] D. Pelloquin[a] and M. Dutheil[b]

[a]Laboratoire CRISMAT (UMR CNRS 6508), ISMRA, 6 Bd du Maréchal Juin, 14050 Caen, France, and [b]Laboratoire SPMS, CNRS-Ecole Centrale Paris, F 92295 Chatenay-Malabry, France

Correspondence e-mail: olivier.perez@ismra.fr

Received 17 April 2001
Accepted 31 October 2001

The structure of the $m = 2$ tubular compound $Bi_4Sr_{12}Co_8O_{30-\delta}$, bismuth strontium cobalt oxide, was determined by single-crystal X-ray diffraction. This phase of orthorhombic symmetry exhibits a very strong tetragonal pseudosymmetry. The structure consists of 90°-oriented $Bi_2Sr_2CoO_{6+\delta}$ slices, four Co atoms wide, forming $[Sr_4Co_4O_{13}]_\infty$ pillars at their intersection. The Co atoms in these pillars form four corner-sharing CoO_5 bipyramids. In the resulting $[Co_4O_{13}]$ cluster, an anionic disorder is evidenced and discussed. Then, an accurate description of the particular structure of the pillars is given. Finally, a comparison with the Mn tubular compound $Bi_{3.6}Sr_{12.4}Mn_8O_{30-\delta}$ is carried out.

1. Introduction

After the discovery of the first tubular phase (Fuertes *et al.*, 1989), a large family of cuprates with the chemical formula $[Bi_2Sr_2CuO_6]_m[Sr_8Cu_6O_{16+\delta}]$ (m = 4, 5, 6 and 7) have been synthesized (Caldes *et al.*, 1991, 1992). These oxides derived from the '2201' structure of the superconducting cuprate $Bi_2Sr_2CuO_6$ (Michel *et al.*, 1987), forming '2201'-type slices which are m octahedra thick, and interconnected through single perovskite-like $Sr_8Cu_6O_{16+\delta}$ ribbons. Based on the ability of manganese and cobalt oxides to accommodate the '2201'-type structure, the Bi–Sr–Mn–O and Bi–Sr–Co–O systems were recently investigated, leading to two new series of tubular oxides, $[Bi_2Sr_2MO_6]_m[Sr_8M_6O_{16+\delta}]$, with M = Mn, Co (m = 2, 4) (Pelloquin *et al.*, 1998, 1999; Masset *et al.*, 1999). Although the structural principles of these oxides are well established, the detailed structure of these compounds is, as yet, not completely understood; depending on the M atom (Co, Mn or Cu), which may exhibit different coordinations, they may involve different oxygen stoichiometries, so that the magnetic and transport properties of these oxides are greatly influenced by oxygen stoichiometry. In this respect, the previous structural study of the m = 2 tubular cobaltite $Bi_4Sr_{12}Co_8O_{30-\delta}$ allows, in a first approach, 90°-oriented $Bi_2Sr_2CoO_{6+\delta}$ slices, four Co (or two Bi) atoms wide, to be evidenced [see Fig. 3 of Pelloquin *et al.* (1999)], forming $[Sr_4Co_4O_{13}]_\infty$ pillars at their intersection. The cobalt environment in these pillars, and in particular the oxygen distribution, could not be understood from the previous HREM and X-ray powder diffraction studies. Moreover, the m = 2 member, $Bi_4Sr_{12}Co_8O_{30-\delta}$, exhibits, with respect to the others, a particular tetragonal symmetry which makes it difficult to understand the actual arrangement of the cobalt polyhedra. The aim of the present single-crystal diffraction study is to shed light on the actual symmetry of this cobaltite and to understand the structure of the $Sr_4Co_4O_{13}$ pillar.

2. Experimental

2.1. Synthesis

Bi_2O_3, SrO_2/SrO and Co_3O_4/Co precursor were weighted in the $BiSr_3CoO_{5.9}$ proportion. To avoid the carbonate contamination, SrO oxide was freshly prepared by heating SrO_2 peroxide at 1275 K. The mixture, intimately ground in an agate mortar, was placed in an alumina finger. This step was performed in a dry box. Next, the mixture was sealed in an evacuated silica ampule and heated to a temperature close to 1175 K at 150 K h^{-1}, kept at this temperature for 24 h, and cooled to room temperature at 150 K h^{-1}.

Pure powder samples of the $Bi_4Sr_{12}Co_8O_{30-\delta}$ phase can be obtained for only $0 \leq \delta \leq 1.2$. This result provides information about the rate of possible oxygen vacancies.

2.2. X-ray diffraction

Needle-shape crystals were chosen and their quality was tested using Weissenberg photographs. One single crystal, exhibiting sharp spots, was selected for the crystallographic study.

The data collection was performed on a Brucker–SMART diffractometer equipped with a CCD camera using monochromated Mo K_α radiation. This wavelength is a good compromise between the spot resolution and the absorption correction. Data were recorded at room temperature. The detector dark current was calibrated before every partial data-collection run (*i.e.* every six hours) to ensure a proper thermal background subtraction from each frame. The diffraction images were also corrected for flood and spatial distortions of the CCD detector. The collected spots were of good quality showing no significant overlap or diffusion streaks. The frame exposure for each region of the Ewald sphere was the result of the best compromise between measuring the weak reflections and not saturating the detector with the strongest spots. To achieve a good redundance, we planned the data collection insuring a good overlap of a large number of equivalent reflections taken with different geometrical configurations of the crystal and of the detector.

The collected frames were integrated with the *SAINT* program (Siemens, 1994), scaled and merged taking into proper account the absorption correction, performed using the crystal shape.

3. Symmetry and refinement

The actual symmetry of the tubular $m = 2$ compound was deduced from the interpretation of Weissenberg camera photographs, electron diffraction patterns and the result of the structural refinement.

The observed symmetry of the diffraction pattern appears to be tetragonal (Laue class: 4/*mmm* or 4/*m*); the refinement of the cell parameters (Table 1), $a \simeq b \simeq 23.48$ Å, $c \simeq 5.52$ Å, $\alpha = \beta = \gamma = 90^\circ$, obtained by centring carefully 25 reflections ($\theta > 25^\circ$) on an Enraf–Nonius CAD-4 diffractometer, leads to identical a and b values within the experimental errors. However, assuming a possible tetragonal pseudosymmetry for the crystals, a phenomenon which has already been observed in some structural-related compounds (Pérez *et al.*, 1997), an orthorhombic symmetry cannot be fully discarded. Unfortunately, a comparison of the internal consistency factors ($R_{\rm int}$) within the possible Laue class 4/*mmm*, 4/*m* and *mmm* does not allow the actual symmetry of the tubular phase to be specified because of analogous $R_{\rm int}$ values. Only a careful structural study including all the possible cases to be refined, as shown hereafter, leads to reliable results.

Table 1
Data-collection details.

Chemical formula	$Bi_4Sr_{12}Co_8O_{30-\delta}$
Crystal size	200 × 60 × 30 μm
Crystal shape	$(\bar{1}00)$ $(0\bar{1}0)$ $(00\bar{1})$ (100) (010) (001)
System	Orthorhombic
Cell parameters (T = 294 K)	a = 23.478 (4) Å
	b = 23.486 (4) Å
	c = 5.5171 (1) Å
Space group	*C*222
Z	4
ρ, μ	6.30 g cm^{-3}, 498 cm^{-1}
Wavelength	0.71073 Å
$(\sin\theta/\lambda)_{\rm max}$	1.14
Number of unique reflections (with $I \geq 3\sigma_I$)	
hkl, $h + k = 2n$	5185
hkl, $h + k = 2n + 1$	295
Internal consistency factor $R_{\rm int}$	
Before absorption correction	0.112
After absorption correction	0.038
Extremal transmission factors	0.05, 0.20
Refinement program	*JANA*2000 (Petříček & Dusek, 2000; Dusek *et al.*, 2001)
Number of refinement parameters	170
Weighting scheme	$1/\sigma_F^2$
$\Delta\rho_{\rm min}$ (e/Å^3)	−5.6
$\Delta\rho_{\rm max}$ (e/Å^3)	5.6
F(000)	4976
Reliability factors (R/$_w R$)	0.059/0.049

Two different sets of *hkl* reflections are observed: $h + k = 2n$ with large intensity and $h + k = 2n + 1$ with very weak intensity, suggesting a strong C pseudotranslational symmetry. This property is also pointed out on Patterson maps where the origin peak and the (1/2, 1/2, 0) peak exhibit quite similar weights.

Considering the C-centred lattice, *i.e.* neglecting the weak reflections, assuming the two possible systems tetragonal and orthorhombic for the crystal, and taking into account that no supplementary extinction condition is observed, the following space groups (SG) are to be tested: *P*4, $P\bar{4}$, *P*4/*m*, *P*422, *P*4*mm*, $P\bar{4}2m$, $P\bar{4}m2$, *P*4/*mmm* (the normal setting for tetragonal symmetry, a = 16.60, b = 16.60, c = 5.5171 Å, $\alpha = \beta = \gamma = 90^\circ$, has been chosen rather than the orthorhombic one, a = 23.478, b = 23.486, c = 5.5171 Å, $\alpha = \beta = \gamma = 90^\circ$) and *Cmmm*, *C*2*mm*, *Cm*2*m*, *Cmm*2, *C*222.

In a first stage, we have considered the different tetragonal space groups. All of them allow the structural model proposed by the HREM study (Pelloquin *et al.*, 1999) to be built. The whole cations can be located in the space groups including a mirror plane perpendicular to x, y or z, only with a splitting out of the mirror for the different atoms. This result suggests that the existence of the mirrors is not consistent with the structural framework. Refinements within the other possible SG

lead to high-reliability R factors ($R > 0.14$); the anisotropic atomic displacement parameters (ADPs) are not defined for both Co and Sr atoms and all of the O atoms cannot be found. These anomalies strongly suggest that the actual symmetry is lower than the tetragonal one.

The first SG checked in orthorhombic symmetry was *Cmmm*. In this preliminary model, Bi and Sr cations sit on special positions on the m_z ($m_z \perp z$) mirror and Co atoms are located both on the m_z and m_x or m_y mirror. However, a strongly elongated ADP normal to the mirror m_z is observed for Bi, Sr and Co atoms. Bearing in mind that the Bi, Co and Sr atoms cannot be distributed at random on both sides of m_z (the Bi—Bi, Co—Co or Sr—Sr distances would be too short), this anomaly suggests that the m_z mirror does not exist, so that the *Cmmm* symmetry is too high. In order to test this hypothesis, the *Cmm*2 SG can be considered.

Starting from the cationic model obtained in the *Cmmm* SG, the atoms have been displaced from their ideal position and their isotropic thermal motion have been fixed to reasonable values. The corresponding shifts have been calculated from the ADPs previously determined. The sign of the displacement was determined by a trial-and-error method for each cation. Within this *Cmm*2 model the previous anomaly is no longer observed and so the hypothesis of a static disorder can be discarded.

At this stage, the thermal displacement of the cations was treated as anisotropic. The structure refinement still indicated some problems for the Co atoms. These atoms, located either on m_x or on m_y, exhibit large ADPs along x or y, respectively. This feature, as discussed in the previous paragraph, suggests the absence of the two orthogonal mirrors. To test this hypothesis, the *C*222 SG has been considered. Within this new SG, the Co atoms exhibit quite reasonable ADPs.

By alternating refinements of the cation coordinates and Fourier difference synthesis, all the O atoms were located, allowing a global refinement of the actual structure to be carried out. The thermal displacements of the cation and the O atoms were treated as anisotropic and isotropic, respectively.

During the latter refinements, we observed that two O atoms, O(17) and O(18), which belong to the $[Sr_4Co_4O_{13}]$ pillar, exhibit a very unusual behaviour. Actually, the Fourier difference maps, including all atoms except O(17) and O(18) (Fig. 1), show that around these positions the electron density spreads over a large distance along **c**. There is no evidence of a splitting of these two atoms on two independent positions; the density seems to be continuous over a long range along **c**. Then, rather than splitting these two atoms, anisotropic ADPs have been introduced for O(17) and O(18) to take into account this phenomenon. Of course, the refined U^{33} ADP must be understood as the signature of a static or dynamic disorder and not as a classical thermal effect. This point will be discussed below.

The occupancy of the cationic sites has been refined and, contrarily to energy-dispersive X-ray spectroscopy analysis previously performed (Pelloquin *et al.*, 1999), no cationic vacancy has been found on the Bi and Sr sites. In particular, the small ADP observed for the Bi atoms is consistent with a full occupancy of these sites. Now, concerning the oxygen sites, owing to both the very weak X-ray sensitivity and the disorder observed in particular for O(17) and O(18), no serious information concerning their occupation can be given. Possible oxygen vacancies, however, cannot be excluded. These parameters have been fixed to unity during the refinement. The agreement factor, corresponding to the refinement in the *C*222 SG, are reported in Table 1 while the atomic positions and thermal parameters are summarized in Table 2. The location of the electronic lone pair [Lp(1) and Lp(2)] for each of the Bi atoms has been obtained using electrostatic equilibrium models (Jakubowicz *et al.*, 1998).

Note that, although the structure of this tubular phase has been solved in a C lattice, the actual symmetry is in fact different, corresponding to the SG *P*222. Indeed, we observed extra reflections (hkl): $h + k = 2n + 1$. Any attempt to refine the structure in a primitive cell failed.

4. Discussion

4.1. About the lowering of symmetry

The clear pseudosymmetry of $Bi_4Co_8Sr_{12}O_{30-\delta}$ is certainly the most crucial point to be understood in solving the structure and is therefore worth accurately quantifying. To this purpose, a structural model was generated from the cations within the tetragonal-enhanced symmetry, starting from the appropriate positions refined in the *C*222 space group, and it was compared with the actual structure. A schematic representation of the cationic positions both in the orthorhombic and in the tetragonal symmetries is given in Fig. 2. The

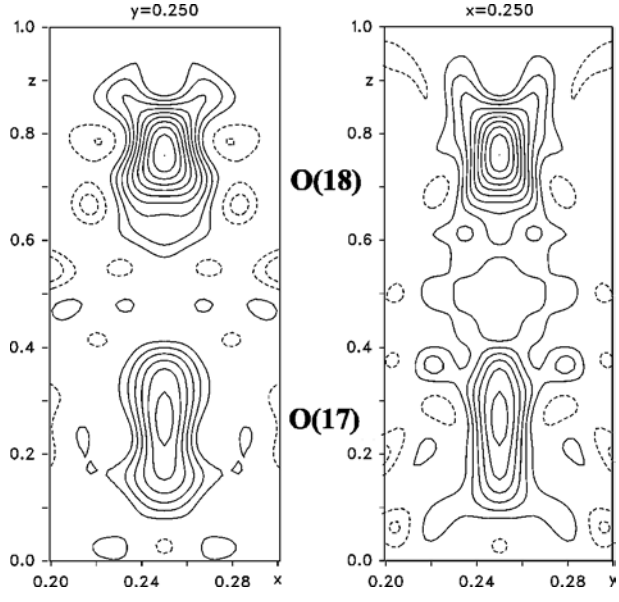

Figure 1
Difference Fourier map showing up the spreading of the electronic density both in the (**ac**) and in the (**bc**) plane for the O(17) and O(18) atoms. Contours are drawn at intervals of 3 e Å^{-3}. Solid lines and short dashed lines represent positive and negative electronic density, respectively.

Table 2
Results of the structure refinement.

An asterisk indicates fixed during the refinement.

	Site	x	y	z	U^{11} or U^{iso}	U^{22}	U^{33}	U^{12}	U^{13}	U^{23}
Bi(1)	8l	0.061551 (9)	0.05578 (1)	0.76886 (7)	0.0068 (1)	0.0060 (1)	0.0079 (2)	0.0002 (1)	−0.0008(2)	0.0003 (2)
Lp(1)	8l	0.0347	0.0389	0.6995	–	–	–	–	–	–
Bi(2)	8l	0.444236 (1)	0.06159 (1)	0.73359 (8)	0.0065 (8)	0.0059 (1)	0.011000	0.0005 (1)	−0.0007(2)	*
Lp (2)	8l	0.4655	0.0390	0.8025	–	–	–	–	–	–
Co(1)	8l	0.16481 (4)	0.24775 (5)	0.2447 (6)	0.0108 (4)	0.0061 (4)	0.0202 (4)	*	−0.007(2)	−0.0022 (5)
Co(2)	8l	0.05601 (4)	0.24203 (5)	0.7537 (4)	0.0068 (4)	0.0214 (5)	0.0074 (5)	0.0012 (4)	−0.0058(8)	0.0043 (5)
Co(3)	8l	0.25214 (5)	0.16459 (4)	0.2622 (5)	0.0069 (4)	0.0099 (4)	0.0174 (6)	−0.0010(4)	−0.0025 (5)	−0.0048(9)
Co(4)	8l	0.25768(4)	0.05616 (4)	0.7470 (4)	0.0223 (5)	0.0061 (4)	0.0083 (5)	−0.0008(4)	0.0047 (5)	−0.0020(8)
Sr(1)	8l	0.05605 (3)	0.16706 (3)	0.2477 (3)	0.0089 (3)	0.0081 (3)	0.0140 (4)	0.0014 (3)	−0.0022(6)	0.0011 (4)
Sr(2)	8l	0.16954 (3)	0.16468 (4)	0.7503 (4)	0.0140 (4)	0.0121 (4)	0.0217 (6)	−0.0021(3)	−0.0031 (6)	0.0008 (7)
Sr(3)	8l	0.17582 (3)	0.05396 (3)	0.2465 (3)	0.0082 (3)	0.0078 (3)	0.0123 (4)	0.0010 (3)	0.0029 (4)	0.0047 (6)
Sr(4)	8l	0.44631 (3)	0.17588 (3)	0.2478 (3)	0.0086 (3)	0.0072 (3)	0.0121 (4)	0.0008 (3)	0.0042 (6)	−0.0009(4)
Sr(5)	8l	0.33519 (3)	0.16952 (4)	0.7561 (4)	0.0139 (3)	0.0133 (4)	0.0195 (6)	−0.0006(3)	0.0015 (6)	0.0021 (6)
Sr(6)	8l	0.33289 (3)	0.05591 (4)	0.2461 (3)	0.0086 (3)	0.0086 (3)	0.0132 (4)	−0.0004(3)	0.0034 (4)	−0.0058(6)
O(1)	4g	0	0.2450 (4)	0	0.010 (3)	–	–	–	–	–
O(2)	4h	0	0.2495 (5)	$\frac{1}{2}$	0.021 (4)	–	–	–	–	–
O(3)	8l	0.1141 (4)	0.2443 (4)	0.006 (2)	0.019 (2)	–	–	–	–	–
O(4)	8l	0.1182 (5)	0.2477 (4)	0.534 (2)	0.025 (2)	–	–	–	–	–
O(5)	8l	0.2512 (4)	0.1107 (5)	0.005 (3)	0.033 (3)	–	–	–	–	–
O(6)	8l	0.2538 (3)	0.1196 (4)	0.525 (2)	0.016 (2)	–	–	–	–	–
O(7)	4f	0.2573 (4)	0	$\frac{1}{2}$	0.009 (2)	–	–	–	–	–
O(8)	4e	0.2521 (4)	0	0	0.011 (3)	–	–	–	–	–
O(9)	8l	0.0561 (2)	0.1472 (2)	0.712 (1)	0.0036 (8)	–	–	–	–	–
O(10)	8l	0.1697 (3)	0.1653 (3)	0.252 (2)	0.020 (2)	–	–	–	–	–
O(11)	8l	0.1505 (2)	0.0547 (3)	0.749 (2)	0.013 (1)	–	–	–	–	–
O(12)	8l	0.5544 (2)	0.1496 (2)	0.250 (2)	0.012 (1)	–	–	–	–	–
O(13)	8l	0.6657 (3)	0.1689 (3)	0.766 (2)	0.022 (2)	–	–	–	–	–
O(14)	8l	0.6475 (2)	0.0561 (3)	0.213 (2)	0.0056 (9)	–	–	–	–	–
O(15)	8l	0.0691 (3)	0.0623 (3)	0.143 (1)	0.012 (2)	–	–	–	–	–
O(16)	8l	0.5617 (3)	0.0702 (3)	0.642 (2)	0.017 (2)	–	–	–	–	–
O(17)	4k	$\frac{1}{4}$	$\frac{1}{4}$	0.25*	0.012 (6)	0.007 (6)	0.50 (4)	−0.006(4)	0	0
O(18)	4k	$\frac{1}{4}$	$\frac{1}{4}$	0.75*	0.024 (5)	0.010 (5)	0.14 (2)	−0.013(4)	0	0

differences Δx, Δy and Δz between the actual coordinates and the ideal ones are summarized in Table 3. The Δx and Δy values are very small, quite similar to the uncertainties, giving rise to an almost perfect fourfold symmetry for the projected structure along **c**. In contrast, the Δz values are significant; the largest ones are observed for the Bi atoms. As a result, the lowering of the symmetry from tetragonal to orthorhombic is mainly due to the stacking mode of the Bi atoms along **c** which exhibit displacements close to 0.095 Å from the ideal tetragonal positions. A similar feature has already been observed for the so-called double collapsed phase, $Bi_{6+x}Sr_{9-x}Fe_5O_{26}$ (Pérez *et al.*, 1997), which also exhibits a pseudotranslational symmetry.

Table 3
Differences between the cation coordinates in the orthorhombic and the tetragonal symmetry.

Atom labels correspond to those of Fig. 2. The values have been multiplied by 10^5.

	Δx	Δy	Δz
Bi(1)[a]	–	–	–
Bi(2)[a]	2 (2)	4 (2)	−3527 (16)
Bi(1)[b]	–	–	–
Bi(2)[b]	−2 (2)	−4 (2)	−3527 (16)
Co(1)[a]	–	–	–
Co(2)[a]	–	–	–
Co(3)[a]	−11 (10)	−22 (8)	1750 (10)
Co(4)[a]	−29 (8)	15 (8)	−670 (8)
Co(1)[b]	–	–	–
Co(2)[b]	–	–	–
Co(3)[b]	11 (10)	22 (8)	1750 (10)
Co(4)[b]	29 (8)	−15 (8)	−670 (8)
Sr(1)[a]	–	–	–
Sr(2)[a]	–	–	–
Sr(3)[a]	–	–	–
Sr(6)[a]	−5 (6)	−14 (6)	−160 (6)
Sr(5)[a]	−13 (6)	−2 (8)	580 (8)
Sr(4)[a]	27 (6)	6 (6)	130 (6)
Sr(1)[b]	–	–	–
Sr(2)[b]	–	–	–
Sr(3)[b]	–	–	–
Sr(6)[b]	5 (6)	14 (6)	−160 (6)
Sr(5)[b]	13 (6)	2 (8)	580 (8)
Sr(4)[b]	27 (6)	−6 (6)	130 (6)

4.2. The bonding scheme

The structure of the $Bi_4Co_8Sr_{12}O_{30-\delta}$ phase is shown in Fig. 3. The Bi and Co environments with nearest oxygen neighbours are shown using both polyhedra and skeletal representations. To clarify the figure, the Sr bonding is not shown.

Two different types of coordination are observed for the Co atoms. Within the '2201' slices the Co atoms labelled Co(2) and Co(4) exhibit quite a similar coordination; the latter can be described as a distorted CoO_6 octahedron. Four strong

bonds with Co—O distances ranging from 1.84 to 1.94 Å define the square plane of the polyhedra; medium and weak apical bonds with distances of 2.24 and 2.53 Å are also involved, leading to distorted elongated octahedra. The bond valence formalism (Brown & Altermatt, 1985) leads to a mean valence state of 2.5 for these Co atoms. The Co(1) and Co(3) atoms, forming the pillars, exhibit a more original coordination involving five strong bonds with Co—O distances ranging from 1.76 to 2.02 Å. The polyhedron defined by the five oxygen neighbours is a bipyramid with a triangular basis. This particular polyhedron has already been evidenced for $Co_2(OH)PO_4$ and $LuFeCoO_4$; the former compound exhibits distorted and edge-sharing bipyramids (Harrison *et al.*, 1995) and the latter shows more symmetric bipyramids quite similar to those observed in the tubular phase (Isobe *et al.*, 1990). A valence state of 2.7 is deduced for the Co(1) and Co(3) atoms.

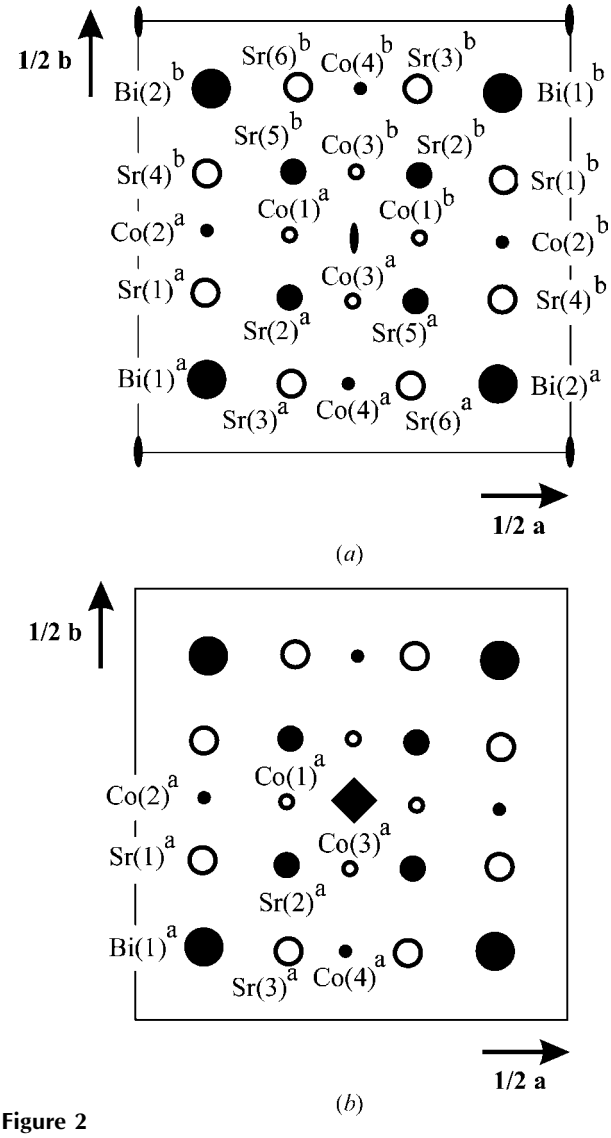

Figure 2
Schematic representation of the tubular $Bi_4Co_8Sr_{12}O_{30-\delta}$ compound in the (**ab**) plane: (*a*) within space group *C*222 (the ^{a} and ^{b} cations are related by the twofold axis $1/2 - x$, $1/2 - y$, z); (*b*) within the tetragonal symmetry (the whole cations are generated from the ^{a} cations by the fourfold axis).

The two bismuth sites have the same type of environment. It is characterized by two Bi—O distances ranging from 2.05 to 2.10 Å and one ranging from 2.15 to 2.20 Å. The O—$\widehat{Bi}$—O angles are close to 90°. Thus, the corresponding coordination polyhedron can be described as a BiO_3L tetrahedron, considering that the electronic lone pair (Lp) of Bi^{III} is directed perpendicularly to the plane defined by the three O atoms. These bismuth environments are similar to those observed in the '2201' cobalt or '2212' copper and iron oxides. Nevertheless, for the modulated compound $Bi_2Sr_2CoO_{6+\delta}$ (Jakubowicz *et al.*, 1999), one of the O—$\widehat{Bi}$—O angles is close to 110°, inducing a smaller distortion of the BiO_3L polyhedron.

The Sr atoms have a ninefold coordination typical of the rock-salt-type structure. The Sr—O distances range from 2.52 to 3.02 Å (Fig. 4).

4.3. The structure of the pillar

The particular arrangement of Co(1), Co(3), O(3), O(4), O(5), O(6), O(10), O(13) and O(17) atoms around the twofold axis passing through the point (1/4 1/4 0) leads to an original structural unit Co_4O_{13} which can be considered as a cluster; it is depicted in Fig. 3. This structural block is built up from four CoO_5 trigonal bipyramids, each polyhedron sharing two edges with its neighbours. It should be noted that the O(17) atom allows the connection among the four CoO_5 polyhedra. Note that the Co—Co distances in those units are rather short (2.8 Å). As shown in Fig. 5, two successive $[Co_4O_{13}]$ units are not directly linked along **c** but are arranged to form a cavity where the O(18) atom is located; this atom plays a particular role in the bonding scheme of the pillar. Contrary to O(17), O(18) does not exhibit any bond with Co atoms but establishes

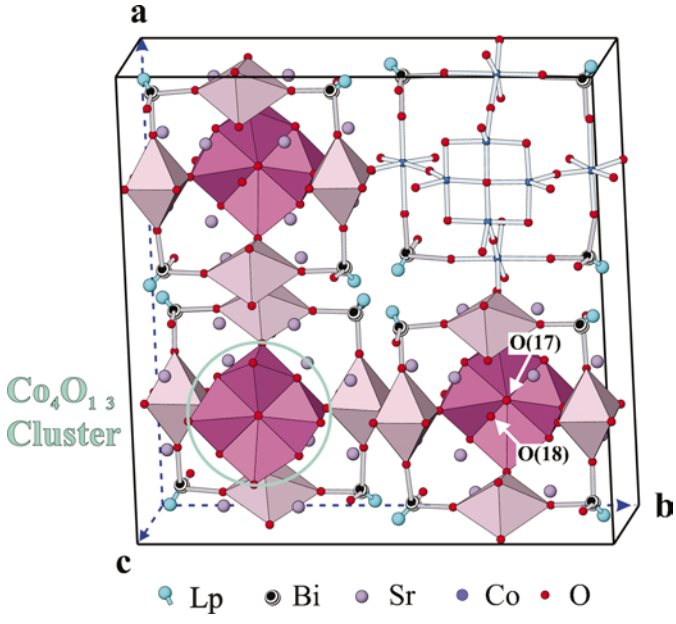

Figure 3
Refined structure of $Bi_4Sr_{12}Co_8O_{30-\delta}$; $[Co_4O_{13}]$ clusters are shown. A quarter of the cell is drawn using skeletal representation to outline the particular configuration of these clusters.

a quite similar bonding scheme with the four neighbouring Sr atoms of types Sr(2) and Sr(5). The corresponding SrO_9 polyhedra are connected to form another cluster of composition $[Sr_4O_{29}]$ (Fig. 4), each polyhedron sharing two triangular faces with its neighbours. As depicted in Fig. 5, two adjacent $[Co_4O_{13}]$ clusters along **c** are then linked through the $[Sr_4O_{29}]$ cluster; SrO_9 polyhedra share some edges with the CoO_5 bipyramids. The regular stacking along **c** of these two structural units gives rise to the formation of the pillars.

Let us consider now the disorder evidenced along **c** for the O(17) and O(18) atoms in §3. An explanation for this disorder is that these O atoms are not located on the ideal positions at z = 1/4 or 3/4 but can be displaced (by up to 0.7 Å) along **z** from this position. This disorder could be static, the distribution of the oxygen positions along **c** inside the compound being then totally stochastic, or dynamic. Then the O(17) and O(18) atoms can occupy a large range of positions along the z axis. Of course, to avoid too short O—O distances, their displacement from the ideal **z** level must be of the same sign for both O atoms. As atoms O(17) and O(18) have only an essential role in the bonding scheme of Co(1), Co(3) and Sr(2), Sr(5) atoms, respectively, a modification of their positions implies mainly a distortion along **z** of the $[Co_4O_{13}]$ and $[Sr_4O_{29}]$ clusters. In fact, in spite of this distortion, these cobalt or strontium units keep their global structural properties (the distances and the angles inside the two types of clusters keep reasonable values whatever the oxygen configurations). Then the O(17) and O(18) atoms appear to have a degree of freedom in the stacking direction of the pillar.

4.4. Comparison with $Bi_{3.6}Sr_{12.4}Mn_8O_{28+\delta}$

The $Bi_{3.6}Sr_{12.4}Mn_8O_{28+\delta}$ compound is the m = 2 member of the Mn tubular family (Pelloquin *et al.*, 1998). It has been previously studied using HREM, X-ray and neutron powder diffraction. Its structure is similar to that of the $Bi_4Co_8Sr_{12}O_{30-\delta}$ phase. However, some interesting differences can be outlined. Considering our present setting [(**a**, **b**) being the pseudotetragonal plane], the tubular Mn phase also exhibits a disorder for the positions of the O atoms within the pillar. Nevertheless, this phenomenon does not appear along the c axis (the stacking direction of the pillar) but in the (**ab**) plane. The O atom corresponding to O(17) in our refinement is, as shown in Fig. 4 of the manganite article (Pelloquin *et al.*, 1998), split into two sites along [110] with an occupancy of 50%. These sites are too close to be occupied simultaneously and the O atom is actually randomly distributed over the two sites. Thus, different configurations can be evidenced for the Mn atoms within the pillar. They are drawn in Fig. 6. The (*a*) and (*b*) configurations are very close; the basis of the Mn pillar can be described by two regular and two distorted bipyramids quite similar to those observed for the $Bi_4Co_8Sr_{12}O_{30-\delta}$ phase. In contrast to the cobalt phase, where each Co bipyramid shares two edges with two adjacent Co bipyramids, each bipyramid in the (*a*) and (*b*) configurations of the Mn phase shares one edge with one bipyramid and one corner with another one. It results, in both cases, in an empty open area between the four polyhedra. These two configurations are oriented at 90° with respect to each other. In the third configuration (drawn in Fig. 6*c*), three different Mn coordinations are involved with two octahedral, one '5 + 1' and one '4' neighbour environments. The two octahedra and the '5 + 1' polyhedron have a common edge. The fourfold coordination of Mn seems to be less realistic; the Mn atom is not located at the centre of the polyhedra but in the middle of one edge. This remark leads us to exclude the latter configuration (Fig. 6*c*) and to assume the existence of the two first configurations (Figs. 6*a* and 6*b*) to explain the disorder observed within the pillar. These structural features are corroborated by HREM studies. As reported above, they outlined for $Bi_4Sr_{12}Co_8O_{30-\delta}$ the existence of a regular cross-shape contrast at the level of the pillar. In the $Bi_{3.6}Sr_{12.4}Mn_8O_{28+\delta}$ compound it is very different; the contrast appears as a diffuse segment, extended alternately along one or the other diagonals of the (001) projection of the pillar. The features explained in the previous

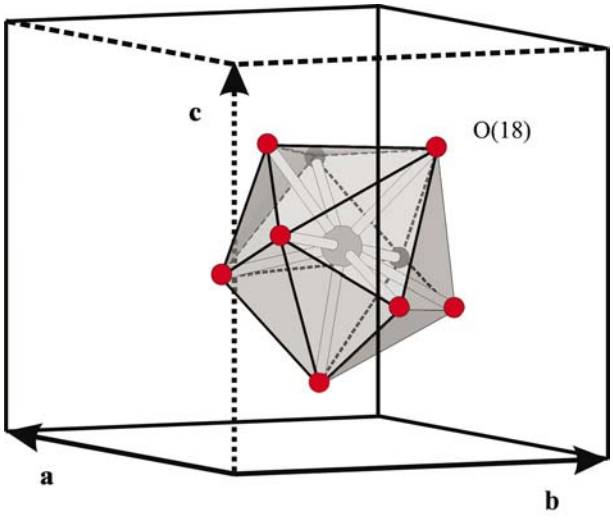

Figure 4
Polyhedral representation of the Sr environment.

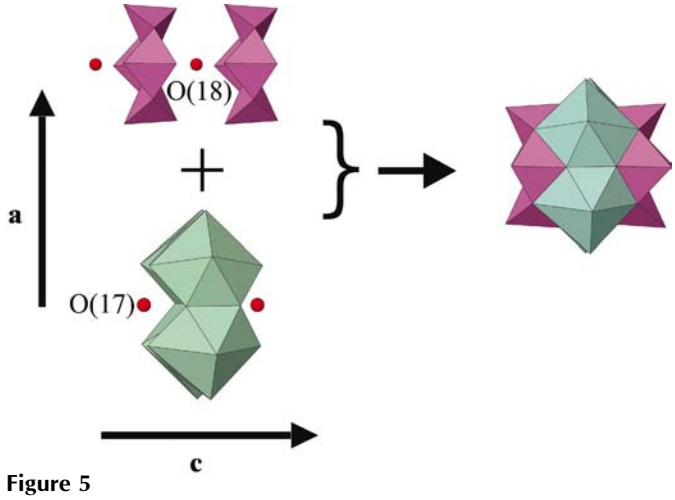

Figure 5
Building scheme of one pillar: regular stacking along **c** of $[Co_4O_{13}]$ and $[Sr_4O_{29}]$ units.

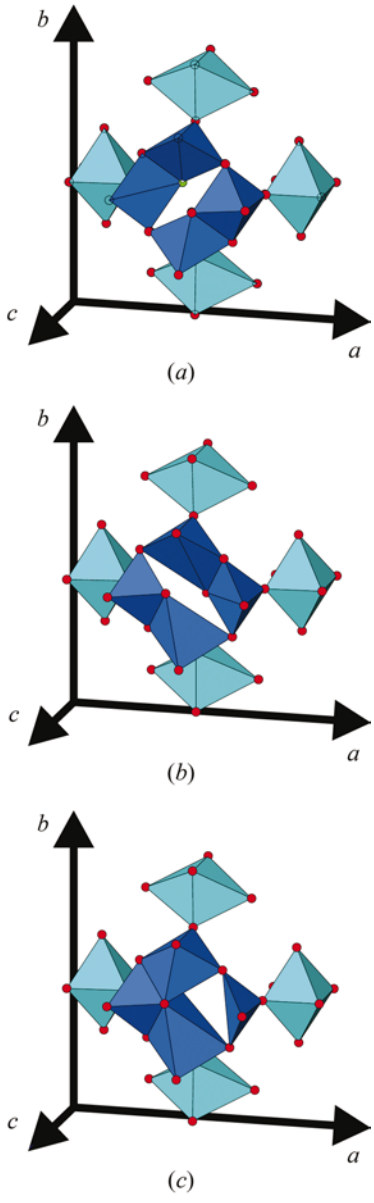

Figure 6
The different possible Mn configurations expected at the pillar level for the manganite $m = 2$ tubular phase $Bi_{3.6}Sr_{12.4}Mn_8O_{28-\delta}$.

paragraph allow us to understand such a phenomenon. Indeed, our refinement does not evidence oxygen disorder within the pillar in the (**ab**) plane. Consequently, the Co_4O_{13} cluster is very symmetric in this plane and the HREM pictures exhibit a regular cross contrast. For the manganite phase, an oxygen disorder in the (**ab**) plane is evidenced; it leads to two different 90°-oriented cluster configurations, inducing the observed contrast.

In conclusion, this study shows that the structure of the $m = 2$ cobalt tubular oxide, although similar to the $m = 2$ manganese phase, differs from the latter by its symmetry, and more importantly by the structure of its $[Sr_4Co_4O_{13}]$ pillars, which exhibit a different oxygen distribution and content.

The authors are indebted to V. Petříček and B. Raveau for helpful discussions.

References

Brown, I. D. & Altermatt, D. (1985). *Acta Cryst.* B**41**, 244–247.
Caldes, M. T., Hervieu, M., Fuertes, A. & Raveau, B. (1992). *J. Solid State Chem.* **97**, 48–55.
Caldes, M. T., Navarro, J. M., Perez, F., Canera, M., Fontuberta, J., Casan-Pastor, M., Miravitlles, C., Obradors, X., Rodriguez-Carvajal, J., Gonzales-Calbet, J., Vallet-Regi, M., Garcia, A. & Fuertes, A. (1991). *Chem. Mater.* **3**, 844–851.
Dusek, M., Petříček, V., Wunschel, M., Dinnebier, R. E. & van Smaalen, S. (2001). *J. Appl. Cryst.* **34**, 398–404.
Fuertes, A., Miravitlles, C., Gonzales-Calbet, J., Vallet-Regi, M., Obradors, X. & Rodriguez-Carvajal, J. (1989). *J. Physica C*, **157**, 525–532.
Harrison, W. T. A., Vaughey, J. T., Dussalk, L. L., Jacobson, A. J., Martin, T. E. & Stucky, G. D. (1995). *J. Solid State Chem.* **114**, 151–158.
Isobe, M., Kimizuka, N., Iida, J. & Takekawa, S. (1990). *Acta Cryst.* C**46**, 1917–1918.
Jakubowicz, N., Grebille, D., Leligny, H. & Evain, M. (1999). *J. Phys. Condens. Matter*, **11**, 3997–4008.
Jakubowicz, N., Pérez, O., Grebille, D. & Leligny, H. (1998). *J. Solid State Chem.* **139**, 194–199.
Masset, A. C., Pelloquin, D., Maignan, A., Hervieu, M., Michel, C. & Raveau, B. (1999). *Chem. Mater.* **11**, 3539–3544.
Michel, C., Hervieu, M., Borel, M. M., Grandin, A., Deslandes, F., Provost, J. & Raveau, B. (1987). *Z. Phys. B*, **68**, 421–423.
Pelloquin, D., Masset, A. C., Maignan, A., Michel, C., Hervieu, M. & Raveau, B. (1999). *Chem. Mater.* **11**, 84–89.
Pelloquin, D., Michel, C., Maignan, A., Hervieu, M. & Raveau, B. (1998). *J. Solid State Chem.* **138**, 278–289.
Pérez, O., Leligny, H., Baldinozzi, G., Grebille, D., Hervieu, M., Labbé, Ph., Groult, D. & Graafsma, H. (1997). *Phys. Rev. B*, **9**, 5662–5672.
Petříček, V. & Dusek, M. (2000). *The Crystallographic Computing System.* Prague: Institute of Physics, Academy of Sciences of the Czech Republic.
Siemens (1994). *SAINT. Data Integration Software.* Siemens Analytical X-ray Instruments Inc., Madison, Wisconsin, USA.